How wrong is collisional Monte Carlo modeling of fast electron transport in high-intensity laser-solid interactions?

J. R. Davies
Instituto Superior Técnico, GoLP, 1049-001 Lisboa, Portugal
(Received 26 April 2001; published 25 January 2002)

The interaction of a high-intensity laser with a solid target generates a large current of fast electrons flowing into the target. Due to the large value of the current, the fast electrons generate significant electric and magnetic fields in the target and rapidly heat it to high temperatures. However, these effects were neglected in interpreting x-ray emission experiments, so the details of the fast electron generation that were inferred could be incorrect. This is considered, theoretically, for layered target, $K\alpha$ emission experiments, by using a hybrid Monte Carlo code that includes field generation. The code is used to model such experiments with aluminum and plastic targets, using fast electron parameters taken from experimental results for average intensities of around 10^{18} W cm^{-2}. These numerical results are then interpreted in the same manner as previous experiments, using only the Monte Carlo part of the code. The field generation leads to lower total emission and to an apparent two-temperature fast electron distribution. The laser absorption into fast electrons inferred by Monte Carlo modeling is consistently lower than the actual value. The mean fast electron energy inferred could be either higher or lower than the actual value, depending on the experimental setup and the cone angle and energy distribution used in the Monte Carlo modeling. The errors caused by neglecting the fields are, in general, greater for plastic than aluminum targets, leading to inconsistencies in results obtained by Monte Carlo modeling.

DOI: 10.1103/PhysRevE.65.026407 PACS number(s): 52.65.Ww, 52.65.Pp, 52.65.Ff, 52.70.La

I. INTRODUCTION

When a high-intensity ($>10^{15}$ W cm^{-2}) laser interacts with a solid target, the solid is rapidly ionized, forming a plasma. The nonlinear laser-plasma interaction leads to the generation of electrons with energies that can significantly exceed both the oscillation energy of an electron in the laser field and the bulk plasma temperature. The study of this phenomenon has a long history and many names; hot, fast, high-energy, superthermal, and suprathermal electrons are all discussed in the literature. We will use the designation fast, because in our theoretical model we consider electrons that are moving much faster than the mean speed of the background electrons. Using this definition, fast electron transport in solids and plasmas has also been extensively studied directly using electron beams, rather than lasers [1,2]. Early studies of fast electrons in laser-plasma physics were largely motivated by their detrimental effect in inertial confinement fusion (ICF) [3–6]. The generation of fast electrons by the compression beams led to preheating of the fuel, reducing the density that could be achieved. It was found that fast electron generation was negligible for $I\lambda^2<10^{15}$ W cm^{-2} μm^2 [6,7], where λ is the laser wavelength, so shorter wavelengths were used. More recently, fast electrons have been studied as a possible benefit to ICF, in the ''fast ignitor'' scheme [8]. This proposes to use the fast electrons generated by a short-pulse laser to rapidly heat the core of a compressed fuel pellet to ignition, before pressure balance is reached. This could lead to far higher energy gain and less stringent symmetry requirements than the conventional technique of driving shocks into the target. This brings us back to earlier work with electron beams [2], where heating plasmas to fusion conditions was also considered. Fast electrons have also been studied because of the x rays and γ rays that they generate [6]. Apart from any specific applications, the generation and transport of fast electrons is fundamental to the study of high-intensity laser-solid interactations, as they are a major factor in the absorption and transport of the laser energy.

The main diagnostic on fast electrons used in laser-solid experiments is x-ray emission. Fast electrons in solids emit x rays directly due to bremsstrahlung and indirectly by exciting atomic transitions. Bremsstrahlung generates a continuous x-ray spectrum, and the gradient of this spectrum has often been used to infer a fast electron temperature [5,7,9,10]. Atomic transitions produce line emission that is characteristic of the emitting element. This has been used to give measurements with spatial resolution by using targets consisting of layers of different materials [3,10–16], and it is this diagnostic that we will concentrate on in this paper. Given the electron energies of interest, the highest energy, $K\alpha$ line emission is used. Typically, the $K\alpha$ emission from 1 or 2 ''fluor'' layers is measured for varying first layer thicknesses, the first layer being that irradiated by the laser. The $K\alpha$ yield as a function of depth is then used to infer the generated fast electron energy distribution and mean energy, the latter being given by the gradient of the curve; the steeper the gradient, the lower the mean energy. The absolute yield can then be used to infer the total fast electron energy, which is normally expressed as the absorption of laser energy into fast electrons. In order to infer these quantities, from both $K\alpha$ and bremsstrahlung emission, the experimental results must be compared to results obtained from theoretical models of the fast electron transport through the target. To model high-intensity laser generated fast electron transport in solids, previous work on the interaction of fast electrons with solids was used. This considered the interaction, or collision,

of single electrons with atoms, electrons, and ions. The most sophisticated of these transport models take the form of Monte Carlo codes. However, the current of electrons generated by a high-intensity laser is far higher than can be obtained with an electron beam, and at these currents the generation of electric and magnetic fields and the heating of the target are significant effects. This has been demonstrated in a number of theoretical studies [17–23], that repeated a lot of previous work on electron beam propagation in plasmas [2], and by many experimental results [14–16,24–29]. This means that collisional interpretations of experimental results are wrong, so the results obtained on the fast electron generation could be wrong. The objective of this paper is to assess these errors for layered target $K\alpha$ emission experiments. To do this, we used a hybrid code that includes field generation in a Monte Carlo code by using Ohm's law to model the response of the target. The code was used to model such experiments and the numerical results were then interpreted in the same manner as previous experiments, using only the Monte Carlo part of the code to infer the mean fast electron energy and absorption of laser energy into fast electrons. These quantities could then be compared with the actual values. The code is described in Sec. II and the details of our numerical experiment in Sec. III. The results are then presented and analyzed using the Monte Carlo part of the code in Sec. IV. The effect of varying some of the more important fast electron parameters is considered in Sec. V and some of the effects that were neglected are considered in Sec. VI. Section VII then gives conclusions and comparisons with experimental results.

II. THE CODE

The code models the transport of a *given* distribution of fast electrons through a uniform solid or plasma (the background). It is assumed that the number density of the fast electrons is very much less than that of the background electrons and that the fast electron velocity is very much greater than the mean background electron velocity. These conditions are clearly fulfilled by high-intensity laser generated fast electrons propagating in solids.

The fast electrons are described by a Fokker-Planck equation. This models the effect of multiple, distant collisions. Collisions between fast electrons are ignored and the background particles are assumed to be stationary, giving only drag and random angular scattering terms. The equation is solved using the equivalent Ito stochastic differential equations [30]. These give the sample paths, or characteristics, of the Fokker-Planck equation, thus providing a formal basis for solving it using particle methods, which are commonly used to solve the Vlasov equation in particle in cell (PIC) [31] codes. In practice, this means that we have computational particles, each representing a specified number of fast electrons, or, more accurately, a specified part of the distribution function, that are moved according to the relativistic equations of motion, with a drag term

$$dp = -\frac{D}{2mv^2}\ln\Lambda_l\, dt, \tag{1}$$

and subject to rotation through a random scattering angle (θ) given by

$$d\theta = \frac{1}{p}\left(\frac{ZD}{v}\ln\Lambda_s\right)^{1/2}\Gamma(t)dt^{1/2}, \tag{2}$$

where p is momentum, $D = n_b e^4/2\pi\varepsilon_0^2$, n_b being the background electron density, e the electron charge, and ε_0 the permittivity of free space, m is the electron mass, v is the electron velocity, Z is the atomic number, dt is the time step, $\Gamma(t)$ is a time varying random number with a Gaussian distribution, mean zero and variance 1, and the logarithmic terms depend on the background material. The equations are solved numerically using explict, first order differencing, in three-dimensional, Cartesian geometry. The random rotation is evaluated using the full cosine and sine terms, as large scattering angles can occur. Equations (1) and (2) tend to infinity as velocity tends to zero, as they only apply to *fast* electrons, so particles whose energy falls below a set value are removed, in effect becoming part of the background electrons. The collisional part of the code is thus a simple Monte Carlo code that neglects large angle scattering and bremsstrahlung, similar to many that have been used in interpreting $K\alpha$ emission experiments.

The background is described by the simple Ohm's law

$$\mathbf{E} = \eta\mathbf{j}_b, \tag{3}$$

where η is the resistivity, which is a specified function of the background temperature T_b, and $\mathbf{j}_b$ is the background current density. In using this equation it is assumed that the background electrons respond instantly to the fast electrons and that their dynamics are dominated by collisions. Substituting this into the Ampere-Maxwell equation and neglecting the displacement current gives the electric field

$$\mathbf{E} = -\eta\mathbf{j}_f + \frac{\eta}{\mu_0}\nabla\times\mathbf{B}, \tag{4}$$

where $\mathbf{j}_f$ is the fast electron current density and μ_0 is the permeability of free space. The first term on the right-hand side of Eq. (4) generates an electric field that opposes the fast electron current. The second term represents the separation of the fast electron and background currents, typically it makes a negligible difference to the electric field on the fast electrons. The equation for $\nabla\cdot\mathbf{E}$ is not used as quasineutrality is assumed. It could be used to find the net charge density, which is assumed to be very much less than that of the background electrons. The magnetic field is given by Faraday's law

$$\frac{\partial\mathbf{B}}{\partial t} = \eta\nabla\times\mathbf{j}_f + \nabla\eta\times\mathbf{j}_f + \frac{\eta}{\mu_0}\nabla^2\mathbf{B} - \frac{1}{\mu_0}\nabla\eta\times\mathbf{B}. \tag{5}$$

The first term on the right-hand side of Eq. (5) generates magnetic field from gradients in the fast electron current density. It acts to increase these gradients, leading to pinching and filamentation. The second term generates magnetic field from gradients in the resistivity, which normally result from heating of the target. If the resistivity increases with tempera-

ture this term generates a magnetic field that enhances the first term, if it decreases with temperature this generates a field with the opposite sign, which acts to push the fast electrons outwards. The third and fourth terms represent diffusion and convection of the magnetic field, respectively. In solving the field equations rotational symmetry is assumed, giving fields $E_r(r,z)$, $E_z(r,z)$, and $B_\theta(r,z)$ that depend only on the radial (r) and axial coordinates (z). The equation $\nabla \cdot \mathbf{B}=0$ is automatically satisfied. Assuming rotational symmetry means that the kink (or hosing, or $m=1$) instability cannot be modeled. Pinching, filamentation, and sausage (or $m=0$) instabilities are included, though filamentation is limited to the formation of concentric cylinders. The field equations are solved on a regular grid, using centered spatial differencing and first order, implicit time differencing. The incomplete Choleski conjugate gradient method is used to solve the resulting five diagonal matrix equation [32]. The fast electron current density on the grid is found by linear weighting from the computational particles to the four nearest grid points, and the fields on the particles are found using the same scheme in reverse, just like an ordinary PIC code [31]. The temperature on the grid is calculated from the energy deposition, found from the Ohmic heating (E^2/η) and the energy loss to collisions of particles in the grid cells, and a specified heat capacity, which may be a function of background temperature. Thermal conduction is neglected. This limits the time scales that can be considered, quite severely so for small spot radii and high fast electron current densities, due both to the high temperatures reached and the occurence of filamentation. The field generation is essentially tacked onto the end of the collisional routines. The electric field is applied to the particles in the same manner as the drag term and the rotation due to the magnetic field in the same manner as that due to the angular scattering. These equations for the fields have been used before to model fast electron propagation in plasmas, in models where the collisions were ignored [2]. Thus we have combined two different, well established, models to give a hybrid code.

III. A NUMERICAL EXPERIMENT

To evaluate the errors that could be caused by ignoring field generation in the interpretation of layered target, $K\alpha$ emission experiments, we used the code to model such an experiment, using parameters taken from experimental results for the fast electron generation. We then interpreted the results from this numerical experiment in the same manner as previous experimental results, using the collisional, Monte Carlo part of the code. The results obtained could then be compared directly with the actual values. In the modeling we made two major simplifications.

(1) Ignore layer effects. Uniform targets were modeled and we calculated what the emission would have been from a series of layers throughout the target. This allowed all the results to be obtained from a single run and avoided infinite gradients in the resistivity between layers [20]. This could be considered as an idealized experiment, as the transport is diagnosed without being affected.

(2) Remove the far boundaries. The boundaries were placed sufficiently far away so that their effect was negligible. This left only the boundary condition at the front surface ($z=0$), where the electrons were generated, to be considered.

Changes in the collision coefficients with background temperature, changes in the $K\alpha$ line energy due to ionization, and excitation of emission by photons were also neglected. These are expected to be relatively small effects. We will now detail the setup of our numerical experiment.

A. Setup

The fast electron generation was calculated from a supposed ''laser'' intensity

$$I=I_p e^{-r^2/R^2} e^{-4(t-t_p)^2/\tau^2}, \tag{6}$$

with peak intensity $I_p=2\times10^{18}\ \mathrm{W\,cm^{-2}}$ spot radius $R=10\ \mu$m, and pulse duration $\tau=1$ ps. The time at which the pulse peaks, t_p, is just a computational parameter, determing at what intensity the fast electron generation is turned on. It was set equal to τ. Similarly, the fast electron generation was turned off after a time 2τ and at a radius of $2R$. It should be stressed that the laser interaction is not modeled, there is *no laser*, just a fast electron beam, thus it is the fast electron current density used that is important, not the precise laser conditions that it may correspond to. An exponential energy distribution ($e^{-K/\langle K\rangle}$) was used with mean energy.

$$\langle K(r,t)\rangle = 0.308[I(r,t)\lambda^2]^{1/3}\ \mathrm{eV}, \tag{7}$$

where K is kinetic energy, I is the intensity from Eq. (6) in $\mathrm{W\,cm^{-2}}$, and λ is the laser wavelength in μm, taken to be 1. The energy distribution was cut off at $4\langle K(r,t)\rangle$. This cut off only affected the results at relatively large depths, which we will not consider. Various fast electron energy distributions are encountered in the literature, for examples see Refs. [3,11,12,15]. No justification can be given for choosing this particular distribution over any other. The effect of varying the distribution is considered in Sec. V. Energy scalings similar to Eq. (7) have been found from numerous experimental results [3,5–7,9,10,12,33]. However, these experimental scalings were based on averaged values from a series of different experiments, whereas we are obtaining a space and time dependent mean energy from a space and time dependent intensity. The overall average energy is

$$\langle K\rangle = 0.168(I_p\lambda^2)^{1/3}\ \mathrm{eV}, \tag{8}$$

which is 212 keV for our parameters. This falls roughly in the middle of the rather wide range of values indicated by the experimental scalings. The number of fast electrons generated was given by

$$N(r,t)=\frac{f_{abs}I(r,t)}{e\langle K(r,t)\rangle}2\pi r\,dr\,dt, \tag{9}$$

with absorption $f_{abs}=0.3$. A wide range of absorption values are given, this value falls roughly in the middle of this range. The fast electrons entered the target from $z=0$ in a random direction within a cone of half angle 30°, having both positive and negative values of radial and azimuthal velocity with equal probability (full solid angle of $4\pi/9$ sr). The cone angle was not determined in most experiments. It is in general agreement with measurements of the cone angle of bremsstrahlung emission [12,29] and radially resolved $K\alpha$ measurements [13]. A fixed number of computational particles were generated each time step with a uniform, random distribution in radius and energy, the desired distribution functions were achieved by varying the number of fast electrons that they represented. To represent continuous generation of fast electrons, the particles were advanced by a random fraction of a time step when they were first generated.

For the targets we used aluminum (Al) and plastic (polyethylene, CH_2). The collisional properties are specified by the density and the logarithmic terms in Eqs. (1) and (2). For $\ln\Lambda_l$ in Eq. (1) we used the term for a cold solid given in Ref. [1]

$$\ln\Lambda_l=\ln\frac{K}{I_{ex}}+\frac{1}{2}\ln(\gamma+1)+\frac{0.909}{\gamma^2}-\frac{0.818}{\gamma}-0.246, \tag{10}$$

where K is the fast electron kinetic energy, $\gamma=1+K/mc^2$ is the Lorentz factor, and I_{ex} is the mean excitation energy, which is 166 eV for aluminum and 57.4 eV for plastic (polyethylene). For $\ln\Lambda_s$ we used an approximate model for angular scattering from atoms given by Joachain [34]

$$\ln\Lambda_s=\ln\frac{4\varepsilon_0 h^2}{Z^{1/3}me^2\lambda_{dB}}, \tag{11}$$

where h is Planck's constant and λ_{dB} is the de Broglie wavelength of the fast electron. For plastic we added the scattering terms for carbon and hydrogen.

For the field generation the target is specified by its resistivity and heat capacity. For the resistivity of aluminum we used an approximate fit to the results of Milchberg *et al.* [35]

$$\eta=\frac{T_b}{5\times10^6+170T_b^{5/2}+3\times10^5T_b}, \tag{12}$$

where T_b is the background temperature in eV. This increases linearly at low temperature, reaches a peak value of 2.2×10^{-6} Ω m at 53 eV, and tends to the Spitzer resistivity, with $Z\ln\Lambda=59$, at high temperature. An initial temperature of 1 eV was used, giving an initial resistivity of 1.9×10^{-7} Ω m. For plastic, we do not have suitable measurements, so we developed a simple heuristic model [15,21] that gives

$$\eta=\frac{1}{4.3\times10^5+1.3\times10^3T_b^{3/2}}, \tag{13}$$

where the initial temperature is taken to be zero, giving an initial resistivity of 2.3×10^{-6} Ω m. At high temperature it tends to the Spitzer resistivity, with $Z\ln\Lambda=7.7$. The basic assumptions of this model are that the initial electrical breakdown is instantaneous and requires a negligible fraction of the fast electrons' energy. For the heat capacity, we used an approximate fit to the heat capacity at constant volume given by the Thomas-Fermi model [36]. Writing it as Cn_b, where n_b is the background electron density, we have

$$C=0.3+1.2T_b'\frac{2.2+T_b'}{(1.1+T_b')^2}, \tag{14}$$

where $T_b'=Z^{-4/3}T_b$ eV. The temperature at the previous time step is used to calculate C. In plastic, the averaged Z (2.67) was used. For low temperatures Eq. (14) gives $C=0.3$ and for $T_b\gg2.2Z^{4/3}$ eV it gives $C=1.5$, the result for an ideal gas.

The computational parameters were; radial grid spacing 1 μm, axial grid spacing 2 μm, time step 1 μm/c, 200 radial and axial grid points, 1500 time steps (5 ps), and 2400 computational particles generated per time step. Particles were specularly reflected from the front surface, allowed to cross the radial boundary (beyond which they generated no fields) and were removed at the far z boundary. The particles were removed when their energy fell below 10 keV.

This leaves only the $K\alpha$ emission to be determined. As we only wish to compare results, an estimate of the relative yield is sufficient, for which we used the energy loss to collisions, given by Eqs. (1) and (10), on the computational grid. To give an idea of how the results would be affected by varying the line energy, we also calculated this using $I_{ex}=20$ keV in Eq. (10).

The main reason for choosing this specific set of parameters was that we have already published results for similar parameters [18–20]. We considered them a sensible choice as there exist extensive, published experimental data for such laser parameters, at significantly lower laser intensities field effects will be negligible, and because there are practical reasons for not considering significantly higher laser intensities. For significantly higher fast electron energies, excitation of $K\alpha$ emission by bremsstrahlung would have to be included. For significantly higher fast electron current densities, thermal conduction would have to be included in order to consider sufficiently long time scales. This also limits the pulse duration that can be considered. A similar reasoning also went into the choice of target materials. A metal and a plastic were also chosen because experimental results show differences between these materials that cannot be explained by purely collisional models [12,16]. Though this was only detected at higher intensities, where we expect the effect of the fields to be greater, in our more precise ''measurements'' any differences should become obvious at a lower intensity.

IV. RESULTS AND INTERPRETATION

The results are given in Figs. 1 and 2, along with the total energy loss and results from runs without fields included, which we will refer to as the collisional results. The results show a series of separate curves, instead of the simple curves of the collisional results, with a rapid initial fall followed by a much slower fall that closely follows the collisional results.

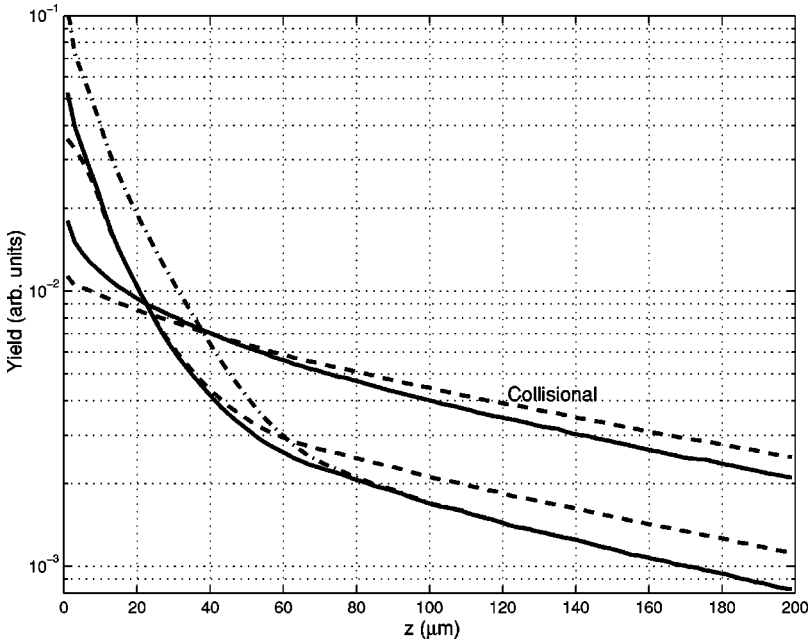

FIG. 1. Model $K\alpha$ yields for aluminum given by the actual energy loss to collisions (solid line) and that calculated with $I_{ex}=20$ keV (dashed line). These results have been normalized to give the same total yields. The dashed-dotted line is the total energy loss. The results labeled collisional were obtained with the fields switched off.

Comparing the total energy loss to the collisional energy loss shows that the sharp initial fall corresponds to the region where the fields dominate, while at large depths the collisions dominate. Although the yields at small depths are much higher than in the collisional results, those at large depths and the total yields are both lower. From these comparisons, we can conclude that collisional modeling of the results will show the following features:

(1) A ''two-temperature'' fast electron distribution.
(2) Lower mean energy than the actual value.
(3) Lower absorption than the actual value.

By two-temperature distribution we mean that we will require two groups of fast electrons with considerably different mean energies to reproduce the separate curves. The steep fall in emission at small depths will give a much lower mean energy than the actual value, while the curves at large depths will give a similar value. To quantify this we used the Monte Carlo part of the code to model the results. As the space and time dependence of the fast electron distribution is now irrelevant, all the fast electrons were generated at the beginning of the runs and at the origin. As the total yield is now proportional to the total fast electron energy, this was set equal to 1. 10^6 computational particles were used and the code was run for 7 ps. Otherwise the setup was the same as described in Sec. III A. We ran the code for a series of mean energies at 5 keV intervals, normalized these results to give the same total yield as the results being analyzed, and found the mean energy that gave the best fit. The absorption was then found from the normalization factor, which gave the total energy of the fast electrons. Fitting the results, consis-

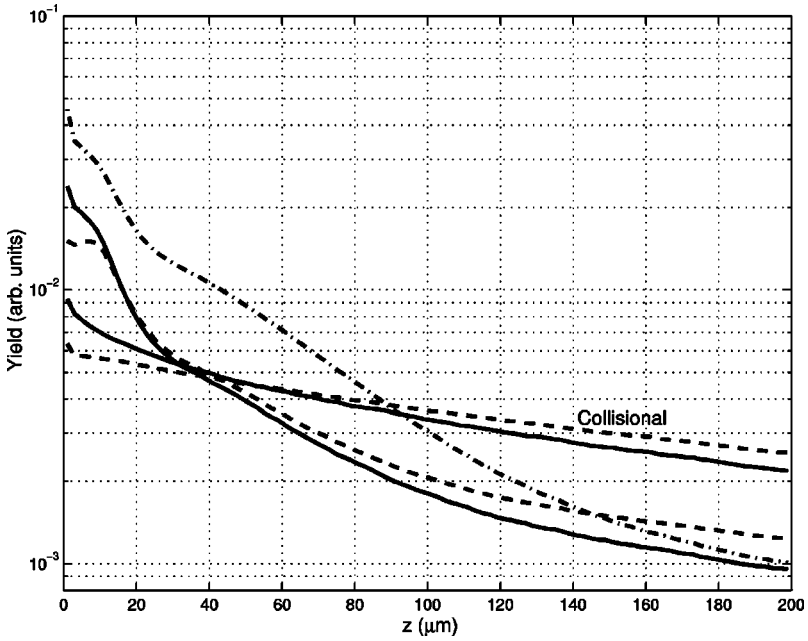

FIG. 2. Same as Fig. 1, but for plastic.

tently, with a number of different fast electron populations is difficult, and such detailed results are also not of much interest, so we just considered results at small and large depths, independently of one another. For small depths, we present results obtained from $z<40\ \mu$m in aluminum and $z<25\ \mu$m in plastic, as these were the greatest depths that could be reasonably fitted by an exponential distribution. For large depths, we present results obtained from $z=100-300\ \mu$m in aluminum and $z=160-360\ \mu$m in plastic, as at these depths the fields are negligible. The results did depend on the region chosen, though very weakly at large depths, so these results should only be considered as estimates of the lower and upper values of mean energy that could be obtained by collisional modeling. At small depths, we obtained a mean energy of 50 keV in both cases and an absorption of 14.3% for aluminum and 11.1% for plastic. At large depths, we obtained a mean energy of 185 keV for aluminum and 170 keV for plastic, and an absorption of 10.9% for aluminum and 11.2% for plastic. The actual values were 212 keV and 30%. The results obtained using $I_{ex}=20$ keV at small depths gave a mean energy of 40 keV and an absorption of 25.9% for aluminum, but the results for plastic could not be well fitted in this region. At large depths, they gave a mean energy of 190 keV for aluminum and 180 keV for plastic and an absorption of 11.1% for both. The results at large depths are similar to the previous ones as both 20 keV and the mean excitation energies are much lower than the mean energy. The significant differences at small depths, where the results are dominated by lower energy electrons, are the first indication of an inconsistency in the collisional modeling. The total absorption that would be obtained from these results is lower than the total of those given above, as the fits were carried out independently of one another. The reduction in the energy lost to collisions is just the energy lost to the electric field, which was 32.2% of the total energy for aluminum and 38.1% for plastic, indicating that total absorptions of 20.3% for aluminum and 18.6% for plastic would be obtained. The total absorption obtained from the results using $I_{ex}=20$ keV would probably be slightly higher. As the yield from the low-energy group is negligible at large depths and that from the high-energy group varies much more slowly with depth, the main difference in fitting consistently with two groups would be to lower the absorption into the low-energy group. Figures of roughly 9.4% for aluminum and 7.4% for plastic would thus be expected. Although the mean energy and total energy of the fast electrons are underestimated, the total number ($\propto f_{abs}/\langle K\rangle$) is overestimated; the number of electrons in just the low-energy group exceeds the actual value, while that of the high-energy electrons is lower. The overall mean energy is reduced by a greater factor than the total energy, or absorption as we have expressed it. However, the apparent two-temperature distribution means that the absorption could be more considerably underestimated than the mean energy. The mean energies obtained from the results at large depths are at most 20% lower than the actual value, while the absorptions are around a third of the actual value. These results also show that field generation has a greater overall effect in plastic than aluminum, only the absorption obtained at large depths was marginally lower for aluminum than plastic. However, this is not the end of the story, because these results were obtained using the same cone angle and energy distribution as used in the original runs, but in a real experiment these are also unknown. To make a more detailed investigation of these, and other effects, we used only the results at large depths.

The cone angle cannot be determined from results at large depths, as the net effect of the angular scattering dominates, so we can only obtain a range of mean energies and absorptions dependent on the cone angle. Cone half angles of 0–90° gave mean energies of 180–210 keV for aluminum and 160–215 keV for plastic, and absorptions of 10.7–11.7 % for aluminum and 11.2–12.7 % for plastic. This uncertainty is only significant for the mean energy, and brings it closer to the actual value. The greater variation in the results for plastic reduces the apparent differences between aluminum and plastic. This occurs as the angular scattering is lower in plastic due to its lower *Z*. Increasing the cone angle significantly increased the yield at small depths, but nowhere near enough to reproduce our results, we would still require a two-temperature distribution.

The energy distribution could be determined from the yield curves of a series of monoenergetic distributions, and repeated for different cone angles or combinations of cone angles. However, in interpreting many experiments, a Maxwellian distribution was assumed and the temperature was given rather than the mean energy, so we will limit ourselves to considering this distribution. However, it depends on the number of dimensions and whether the relativistic form is used. The relativistic Maxwellian energy distribution in N dimensions is

$$f(K)\propto\gamma(\gamma^2-1)^{N/2-1}e^{-K/kT}, \tag{15}$$

where $\gamma=1+K/mc^2$ and kT is temperature. In the nonrelativistic limit $K\ll mc^2$, this tends to $K^{N/2-1}e^{-K/kT}$, and in the ultrarelativistic limit $K\gg mc^2$, to $K^{N-1}e^{-K/kT}$. The mean energy of a distribution of the form $K^ne^{-K/kt}$ is $(1+n)kT$. In the nonrelativistic limit $kT\ll mc^2$, this gives the classical law of equipartition of energy, $\langle K\rangle=NkT/2$. In the ultrarelativistic limit $kT\gg mc^2$, this changes to $\langle K\rangle=NkT$. For intermediate temperatures, the mean energy lies between these two extremes. If the type of Maxwellian is not clarified, this gives a wide range of possible values of mean energy for a given temperature. Our exponential distribution is now seen to be a two-dimensional, nonrelativistic Maxwellian and a one-dimensional, ultrarelativistic Maxwellian. Given the mean energy used, it would be best described as a two-dimensional Maxwellian. Its temperature is equal to its mean energy, so in this case the terms are interchangeable. To see the effect of using such distributions on the mean energy obtained, we ran energy distributions of the form $K^ne^{-K/kT}$, with n equal to $-1/2$, 0, 1/2, 1, 3/2, and 2, for aluminum targets with a cone angle of 30° and a mean energy of 185 keV, the value that gave the best fit for $n=0$ (exponential). The results at large depths were broadly similar, except for $n=-1/2$, where a temperature of 185 keV, that is, a mean energy 92.5 keV, was clearly much closer. Some of these

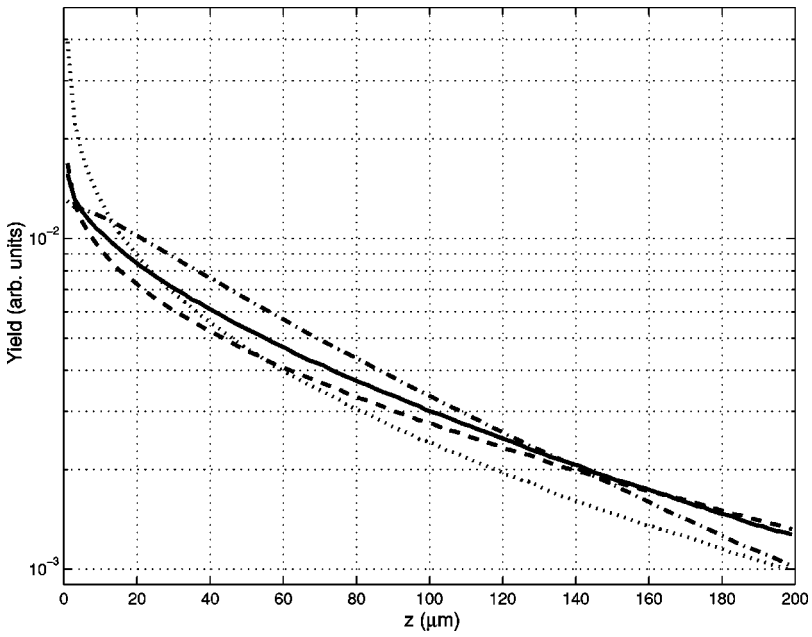

FIG. 3. Yields, given by the energy loss to collisions, for aluminum from collisional runs using energy distributions given by $K^n e^{-K/kT}$ with $n=-1/2$ (dotted line), $n=0$ (dashed line), $n=1/2$ (solid line), and $n=2$ (dashed-dotted line), for a mean energy of 185 keV, except for $n=-1/2$, which has a temperature of 185 keV (mean energy 92.5 keV).

results are given in Fig. 3. The gradients at large depths increase with n, so a higher value of n would give a higher mean energy, but a lower temperature. We investigated $n=1/2$ (three-dimensional, nonrelativistic Maxwellian) in more detail. For cone half angles of 0–90°, this gave mean energies of 220–255 keV (kT of 147–170 keV) and absorptions of 9.83–10.8 % , compared to 180–210 keV and 10.7–11.7 % obtained with $n=0$. This shows that the energy distribution can significantly affect the mean energy obtained, while having a relatively small effect on the absorption, as noted by Hares *et al.* [3]. The $n=1/2$ distribution gave a better fit than the original exponential distribution. To determine which of the energy distributions would give the best fit, we fitted the curves at large depths with the function $\exp(-(z/z_0)^{\alpha})$, taken from the results of Harrach and Kidder [37] and Wienke [38]. According to these results, and ours, we expect the value of α for a given material to depend largely on the energy distribution, remaining roughly constant over a wide range of mean energies and cone angles. For $n=-1/2$ to 2 we obtained values of α (to two significant figures) of 0.47, 0.55, 0.63, 0.73, 0.82, and 0.82. The function was a good fit in the region considered (100–300 μm), but did not fit well at small depths (typically $z<z_0$). From the full results for aluminum, we obtained a value of 0.69, closer to the result for $n=1$ than $n=0$. Fitting with $n=1$ would give a significantly higher mean energy, and a lower temperature, than obtained with $n=0$. For plastic, we obtained 0.90 compared to 0.69 from the collisional result, also indicating that a higher value of n, and hence a higher mean energy, would give a better fit. The main difference between the indicated energy distribution and the original exponential distribution is that it contains far fewer electrons at low energies. For $n>0$, the distribution peaks at nkT and is zero at zero energy, while for $n\leqslant 0$, the distribution peaks at zero energy. It is this lack of lower energy electrons that gives a higher mean energy, the results do not indicate that the fields have increased the apparent energy of the electrons. This changes our initial conclusions, the mean energy could be overestimated. However, the temperature obtained is lower, and it is often this that is quoted. We use mean energy as this is the important factor in determining the field generation and its meaning is clear, whatever the distribution. Temperature is only a meaningful parameter in the context of a particular Maxwellian distribution. This is also true of the term two temperature, for example, if you interpreted the results for $n=-1/2$ (Fig. 3) using any of the other distributions you would require two temperatures. However, our results would require two temperatures, whichever of these distribution was used. The overall energy distribution indicated by our results has two distinct peaks, rather than two different gradients. The effect of varying the energy distribution in the full runs is considered in Sec. V.

Another factor that affects the collisional modeling is the boundary condition. The electrons were specularly reflected at the front surface, as they were in the full runs. Removing the electrons gave, for cone half angles of 0–90°, mean energies of 175–195 keV for aluminum and 160–195 keV for plastic, compared to 180–210 keV and 160–215 keV obtained previously, and absorptions of 11.1–14.5 % for aluminum and 11.1–14.3 % for plastic, compared to 10.7–11.7 % and 11.2–12.7 % obtained previously. The total absorptions now varied with the cone angle, as energy was escaping from the boundary, and were 20.5–25.6 % for aluminum and 18.1–21.6 % for plastic, compared to 20.3% and 18.6 % obtained previously. This is the only factor we have considered that has a significant effect on the absorptions, increasing the values obtained for large cone angles. The reduction in the mean energy is not significant. As the effect is greater for aluminum, due to its higher Z, the differences between aluminum and plastic are significantly reduced by removing the electrons at the boundary. The effect of removing the electrons at the boundary in the full runs is considered in Sec. V.

Of the two extreme cases that we have considered, that is, the results at small and large depths, only the last case corresponds to any actual $K\alpha$ emission experiments. In real experiments, the emission at small depths is often not measured, the fluor layers are much thicker than 2 μm, fewer points are obtained, and there are normally considerable error bars on the results. This would tend to hide the distinct curves seen in our results, thus a two-temperature distribution would not necessarily be obtained and the results could lie somewhere between these two extremes. The experiments that would be most affected by the emission at small depths, and thus would give the lowest mean energy, are those that used two fluor layers without a first layer. As an example, we considered the yield from a first fluor layer of 50 μm and a second fluor layer of 100 μm in aluminum for $I_{ex} = 20$ keV, based on the type of set up used by Beg *et al.* [10]. For an exponential energy distribution, a cone angle of 0 gave a mean energy, determined from the ratio of the yields, of 70 keV and absorptions of 22.3% and 21.2% determined from the yields of the first and second layers, respectively. A cone half angle of 90° gave a mean energy of 85 keV and absorptions of 19.9% from both layers. This gives a mean energy close to the lower limit and an absorption close to the total value given above. In this case, the increased emission at small depths can be accounted for by a large cone angle instead of a two-temperature distribution. The use of the $n=-1/2$ distribution considered above (Fig. 3) would probably account for this with a somewhat smaller cone angle. These less precise measurements lead to a greater uncertainty as to the fast electron distribution.

To summarize, we have found that by varying the target material, the line energy, the region of the measurements, and the assumptions used in the collisional modeling (cone angle, energy distribution and boundary condition), we can obtain mean energies of 50–255 keV and absorptions of 10–26% from original values of 212 keV and 30%.

We will now attempt to understand these results in terms of the effect of the fields on the fast electrons. If we followed electrons that were travelling against an electric field that we did not know about, we would conclude that they had a lower energy. However, we would get the number of electrons right, the total and mean energies would fall by the same factor. The effect of the electric field could be simply summarized by the energy loss to the field, which was 32.2% for aluminum and 38.1% for plastic, but this only applies to the total absorption. The apparent mean energy of the electrons is further reduced by the magnetic field, without lowering the total energy, as it reduces an electron's penetration depth by increasing the curvature of its trajectory. This effect is greater, the lower an electron's energy; electrons with a low enough energy are turned around by the magnetic field, while electrons with a much higher energy can even have their penetration depths increased, as the field can reduce their initial angle to the axis. The folding up of electron trajectories by the magnetic field can only be accounted for in collisional modeling by a larger number of much lower energy electrons. This is the origin of the two-temperature distribution. The apparent mean energy at large depths is increased and the absorption decreased because lower energy electrons are turned back by the magnetic field. The magnitude of this effect can be seen from the number of electrons returned to the front surface. In aluminum this was 49.3% of the total number generated, accounting for 37.8% of the total energy, compared to 16% and 8.1%, respectively, for the collisional run (backscatter due to angular scattering). In plastic, 22.5% of the electrons and 11.4% of the energy returned to the front surface, for the collisional run the figures were 3.8% and 1.5%, respectively. This, roughly, factor of two difference between aluminum and plastic is also seen in the maximum values of the magnetic fields of 1.30 kT (13 MG) and 0.627 kT (6.27 MG), respectively. This explains the smaller differences between the results obtained for aluminum and plastic than indicated by the energy loss to the electric field. It is not correct to simply state that the effect of the fields is greater in plastic than in aluminum, it is different. The magnetic field greatly complicates the situation, as its effect cannot be so simply quantified as that of the electric field and it is far more sensitive to the parameters used. Clearly, the boundary condition is one of these parameters, and we investigate this in Sec. V. To confirm this simple explanation we reran the aluminum run with the magnetic field switched off. It did indeed give a curve that could be accounted for by a single temperature, with the reduction in mean energy and absorption both adequately accounted for by the energy loss to the electric field.

The reason for the magnetic field being much higher in aluminum than in plastic is that its resistivity initially increases with temperature. In terms of Eq. (5), the second term on the right-hand side is enhancing the first term. In terms of the currents, there is a more rapid separation between the fast electron and background return currents, as the background current can more readily flow in the colder, lower resistivity region around the fast electron beam. The continual fall in resistivity with temperature in plastic, and that at high temperatures in aluminum, has the opposite effect. It leads to the background return current concentrating on the axis and the fast electron current in an annular region around it. It also lowers the electric field, but to a far lesser extent, the maximum electric field in plastic was 10.9 $\mathrm{GV\,m^{-1}}$ compared to 13.0 $\mathrm{GV\,m^{-1}}$ in aluminum. It should be remembered that their maximum resistivities were very similar. The electric field is far less affected by where the return current flows, because whatever it does, the energy required to drive it must come from the fast electrons. The overall effect of the electric field was lower in aluminum as field generation only became important when it began to heat up, which initially occurred due to collisions, whereas in plastic the fast electron propagation depended on heating the target. This can be seen in the much more rapid convergence of the total energy loss with the collisional energy loss in aluminum, Fig. 1, than in plastic, Fig. 2. In plastic, the difference between the total energy loss and the collisional energy loss initially increases with depth, before eventually falling, leading to a more complex series of curves than for aluminum. This is because the fall in resistivity due to Ohmic heating led to the electric field falling with increasing

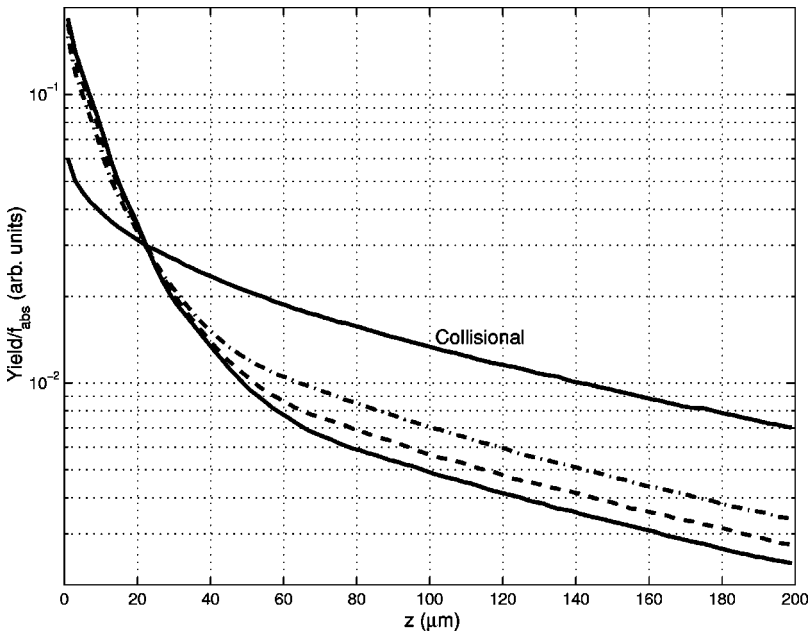

FIG. 4. Yields, given by the collisional energy loss, divided by the absorption for aluminum and absorptions of 20% (dashed-dotted line), 30% (dashed line), and 40% (solid line). The result labeled collisional was obtained with the fields switched off, it is independent of absorption.

fast electron current density [21]. This also occured in aluminum, but not to a sufficient extent to affect these radially and time integrated results.

The effect of the fields may have been underestimated in plastic at large depths, as the resistivity we used [Eq. (13)] assumed that the initial electrical breakdown required a negligible fraction of the fast electron energy. For the lower fast electron fluxes at large depths, this is not a good approximation. The fast electron flux that can propagate without breaking down the plastic is, for our purposes, negligible. This could lead to a sudden fall in emission at large depths.

V. FURTHER EXPERIMENTS

We will now consider the effect of varying the fast electron generation and the boundary condition in the full runs. As we only wished to establish general trends, we only considered aluminum targets and the yield given by the collisional energy loss, comparing the results to the previous results, rather than making further extensive analyses.

For the field generation, the most important parameter of the fast electrons is their current density, which is proportional to $f_{abs}I/\langle K\rangle$. To change this directly without altering the collisional effects, we varied the absorption, considering values of 20% and 40%, in addition to the original 30%. The collisional energy losses divided by the absorptions are given in Fig. 4, the collisional results are identical as they are proportional to the absorption. The only significant change in the results with absorption is in the total emission at large depths, which falls with respect to the collisional result as absorption increases. The energy loss to the electric field was 28.4%, 32.2%, and 34.2% for absorptions of 20%, 30%, and 40%, respectively, indicating that total absorptions of 14.3%, 20.3%, and 26.3% would be inferred. The mean energies inferred at small depths would be slightly lower, the higher the absorption, but those obtained at large depths, by fitting with an exponential energy distribution, were almost identical, only the absorptions changed. For cone half angles of 0–90°, absorptions of 8.89–9.58 %, 10.7–11.7 %, and 12.3–13.4 % were obtained, which represent reductions from the actual values of 56–52 %, 64–61 %, and 69–66 %. However, the functional form of the curves did change, fitting the results with the function $\exp(-(z/z_0)^{\alpha})$ (Sec. IV) in the collision dominated region gave values of α of 0.65, 0.69, and 0.85. Fitting with the indicated energy distribution would thus give higher mean energies at higher absorptions. These results show that we are in a regime where the field effects increase with increasing current density, however, the overall effects of the fields are not directly proportional to the absorption. In doubling the absorption from 20% to 40%, the energy loss to the electric field only increased by a factor of 1.20, and the maximum magnetic and electric fields by factors of 1.10 and 1.24, respectively. This shows us that the eventual reduction in the resistivity due to target heating is having a significant effect. The relatively weak variation in the results with the fast electron current density means that the results obtained here will be typical of a wide range of parameters.

Another factor that could affect the results, but that does not alter the generated current density, is the energy distribution. We considered a $K^{1/2}e^{-K/kT}$ (three-dimensional, nonrelativistic Maxwellian) energy distribution with the same mean energy [Eq. (7)] as before. For this run, the energy distribution was cut off at $9\langle K\rangle$ $(6kT)$ instead of $4\langle K\rangle$, as it does not fall off so rapidly. The results are given in Fig. 5. They show the same features as the previous results. The overall effects of the fields were not significantly changed, the energy loss to the electric field was 33.6% compared to 32.2% for the exponential distribution and the number of electrons returned to the front surface was 51.4%, accounting for 41.0% of the energy, compared to the previous 49.3% and 37.8%. The maximum magnetic field was identical, but the maximum electric field was 50% higher. The energy loss was similar as it was maintained for a shorter time, the magnetic

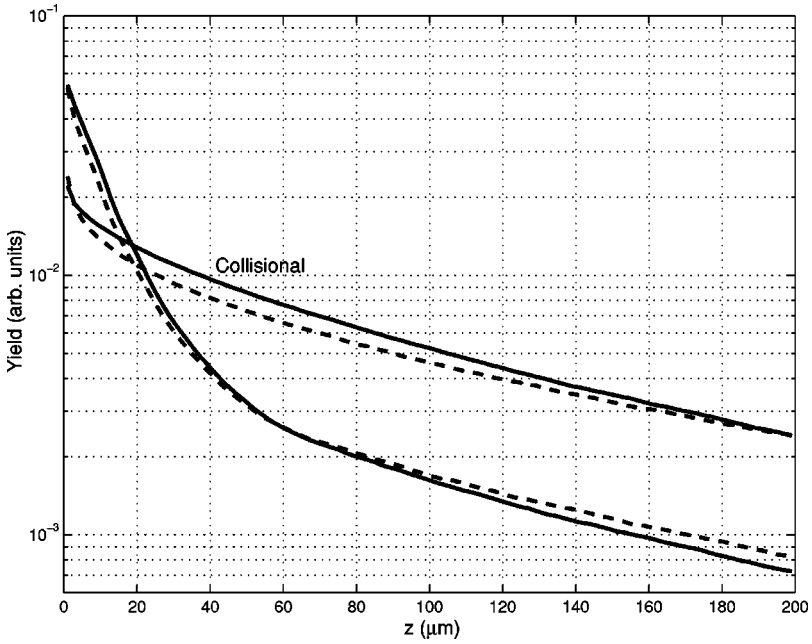

FIG. 5. Yields, given by the collisional energy loss, for aluminum using a $K^{1/2}e^{-K/kT}$ energy distribution (solid line) and an exponential energy distribution (dashed line) with the same mean energies. The results labeled collisional were obtained with the fields switched off.

field also changed more rapidly in time. The differences are due to the lack of low-energy electrons in this distribution, which are readily turned around by the magnetic field to form part of the return current. Fitting the yield at large depths using a $K^{1/2}e^{-K/kT}$ distribution and cone half angles of 0–90° gave mean energies of 200–230 keV (kT of 133–153 keV) and absorptions of 9.20–10.1 %. For the exponential distribution fitting with the original distribution gave 180–210 keV and 10.7–11.7 %. The value of α obtained was 0.61, compared to 0.63 for the collisional run, for the exponential distribution the value was 0.69, and 0.55 for the collisional run. The energy distribution indicated at large depths is not significantly different from the original distribution and has a slightly lower mean energy, quite unlike the results obtained with the exponential distribution. However, the changes this indicates in the energy distribution inferred at large depths are the same; removal of low-energy electrons and a slight reduction in the energy of high-energy electrons.

In Sec. IV, we saw that a significant fraction of the fast electrons was returned to the front surface by the magnetic field, the effect being most significant for aluminum. This means that the reflective boundary has a significant effect, so we considered the effect of removing the electrons instead of reflecting them. For this run, 4000 computational particles were generated per timestep. The results are given in Fig. 6. They show the same features, but the yield is much lower; 42.0% of the energy escaped and 17.9% was lost to the electric field, compared to the 32.2% lost to the electric field when the electrons were reflected. As a fraction of the energy that remained in the target, the energy loss to the electric

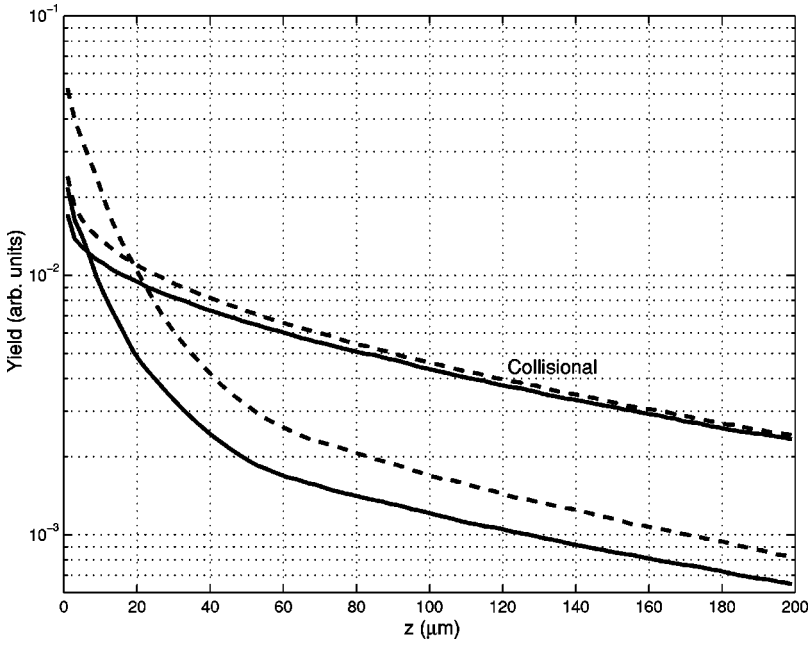

FIG. 6. Yields, given by the collisional energy loss, for aluminum with electrons removed at the front surface (solid lines) and reflected (dashed lines). The results labeled collisional were obtained with the fields switched off.

field was greater. This indicates that a total absorption of 12.0% would be obtained, compared to the previous 20.3%. The yield has steeper gradients, so the mean energies inferred would be higher. Fitting an exponential energy distribution to the results at large depths for cone half angles of 0–90°, and still reflecting the electrons at the boundary, gave mean energies of 215–260 keV and absorptions of 7.82–8.74 %, compared to 180–210 keV and 10.7–11.7 % obtained before. As we saw in Sec. IV, removing the electrons at the boundary in the collisional modeling would slightly reduce the mean energy and increase the absorption at large cone angles. The value of α obtained was 0.61, as before, so the same energy distribution would be inferred from the yield at large depths. Thus, the mean energy would, in general, be overestimated from results at large depths, but still significantly underestimated from results at small depths. As the lower energy electrons turned around by the magnetic field are now lost, the total emission is reduced and the mean energy of the electrons in the target is increased. The maximum magnetic and electric fields were increased by factors of 1.60 and 1.32, respectively, this appears to be due to the lower heating resulting in a higher resistivity. The boundary condition is thus the most significant of the effects we have considered so far and, therefore, merits deeper consideration. For an isolated target in vacuum, all but a small fraction of the highest energy electrons would be reflected by the electrostatic field generated, though with some energy loss to ion motion [17]. Only when there is an extensive plasma on the front surface, due to a prepulse or a long pulse duration, would we expect the removal of electrons to be a reasonable approximation. In this case, the transport of the fast electrons in the plasma should be modeled. However, the majority of electrons that returned to the front surface did so within the assumed spot radius and pulse duration; by the peak of our supposed laser intensity [Eq. (6)] 23% of the energy deposited had left the boundary and by the time the fast electron generation was turned off, the value had reached 41%. Thus, most of the fast electrons returned to the front surface would reinteract with the laser, and this interaction would determine the boundary condition. The fast electron generation and transport in the solid target cannot be separated. However, this separation is dictated by what is computationally possible, not by physics.

VI. OTHER EFFECTS

We will now briefly discuss the two effects that we neglected right at the beginning in Sec. III, layer effects and the far boundaries.

The most significant effect of layers in terms of the field generation is that they introduce infinite gradients in the resistivity. This will lead to the generation of magnetic field at the interface from the $(\nabla \eta)_z (j_f)_r$ term in Eq. (5), that is, fast electron flow parallel to the interface will lead to a growing magnetic field at the interface. The magnetic field will not in fact be infinite, as its scale length will be determined by magnetic diffusion. However, the factor that determines the importance of the magnetic field is the ratio of the Larmor radius of an electron to the scale length of the magnetic field, and this is independent of the scale length, so this does not have to be considered. Such an approach was taken by Bell *et al.* [20], who showed that this magnetic field could be significant, and comparable to that generated by gradients in the fast electron current density. However, the code cannot represent an infinite gradient, it would be determined by the grid spacing. Whether the effects just mentioned will lead to the overall effect being independent of the grid spacing has yet to be fully investigated.

So far we have only considered the boundary condition at the front surface, which could not be avoided as this is where the fast electrons entered. Targets used in experiments are typically wide enough that the edges, or radial boundary in the code, can be reasonably ignored, and as this presents no technical problem we will not consider it. However, in practice, the target cannot be made so thick that the rear surface can be ignored, as the emission is normally measured from the back of the target. The same basic considerations apply to this boundary as to the front surface discussed in Secs. IV and V. In collisional modeling, removing the electrons would lead to a lower yield and to a steeper gradient in the yield curve than reflecting them, and hence to a higher absorption and a higher mean energy being inferred, the effect being greatest for the absorption. As the energy reaching the rear surface can readily exceed that returned to the front surface by angular scattering, this boundary condition could be a major factor in determining the absorption in collisional modeling, and this has indeed been found to be the case [11]. For the full runs, the situation is more complicated, as reflecting the electrons will change the field generation due to the interaction between the incident and reflected currents. In Ref. [21], for 70–250 μm thick plastic targets and an intensity ten times higher than that used here, we reported that either specular or diffuse reflection of the electrons led to the incident electrons being pinched and the reflected electrons being forced outwards by the self-generated magnetic field. The energy deposition immediately behind the rear surface was considerably enhanced, while the results in the bulk of the target were unaffected. The reflected electrons did not freely recirculate as in the collisional case. If the emission near the rear surface was not measured, this would lead to the absorption being significantly underestimated in collisional modeling, if the electrons were also reflected. In this case, removing the electrons would give more accurate results. For significantly thinner targets, the interaction between the forward and reflected fast electron currents would be much stronger, and quite different results could be expected. This has not yet been investigated. To give an idea of what thin and thick mean in our case, we considered the cumulative, total energy deposition as a function of depth. Half of the energy was lost over a distance of 12 μm in aluminum and 32 μm in plastic, so for targets of this thickness or less, we expect the results to be dominated by the rear boundary. 90% of the energy was lost over a distance of 140 μm in aluminum and 180 μm in plastic, so for targets of this thickness or greater, we expect the results to be relatively unaffected by the rear boundary. The effect of the target thickness is further complicated as emission curves in real experiments are obtained from a series of different targets,

whose thicknesses may vary. Furthermore, the target thickness may affect the fast electron generation, not just because of its effect on the transport, but because electrons reflected from the rear surface could reinteract with the laser. This makes it difficult to draw general conclusions.

VII. CONCLUSIONS

Collisional Monte Carlo modeling of fast electron transport in high-intensity laser-solid experiments is incorrect due to the neglect of field generation and, therefore, it will give inaccurate results on fast electron generation in the interpretation of experiments. It is also incorrect to treat the target as a cold solid, as it is rapidly heated to high temperatures by the fast electrons.

Our results show that collisional Monte Carlo modeling of layered target, $K\alpha$ emission experiments can reproduce the results, even if field generation is significant. The energy loss to the electric field reduces the apparent energy of the electrons, reducing the mean energy and absorption inferred, while not affecting the apparent number of electrons. The reduction in penetration depth by the magnetic field lowers the apparent energy and increases the apparent number of electrons. This effect is far greater, the lower an electron's energy, leading to an apparent separation of the energy distribution into two distinct peaks; a two-temperature distribution. This means that the absorption inferred can be even further reduced and the mean energy can be either under estimated or overestimated. The exact errors will depend on the experimental setup and the assumptions used in the modeling. Taking experimental results on fast electron generation as a whole, we expect the actual mean energy to fall within the range of values indicated and the absorption to be at the higher end of the range of values indicated. Scalings of fast electron mean energy with intensity established from many different experiments should not be significantly in error, at least for cases where the field generation is comparable to or less than that for those considered here. This can be assessed from the results presented here.

The neglect of field generation will have a similar effect on the interpretation of bremsstrahlung emission measurements, as bremsstrahlung is largely caused by angular scattering of fast electrons. The accelerations caused by the fields are negligible in comparison. The effect should be less than on $K\alpha$ emission as the magnetic field will only affect the direction of the emission, not the apparent energy and number of the electrons. However, it could lead to an apparent low temperature, isotropic emission and a higher temperature, beamed emission, though with a broader cone angle than in the collisional case [29]. This, of course, depends on the boundary condition, if the electrons escaped or lost energy on reflection at the front surface, the magnetic field would lower the total energy and change the energy distribution of the electrons in the target. Beg *et al.* [10] reported higher mean energies from bremsstrahlung measurements than from layered target, $K\alpha$ emission measurements, as might be expected, however, they mention that this could be due to differences in the laser conditions for the different experiments.

Although any individual result maybe reproduced by collisional modeling, the importance of field generation could be inferred from a number of different results, as the results obtained for identical fast electron sources would vary with the target material and line energy used. However, for the cases we considered, these differences were negligible compared to the uncertainties in the Monte Carlo modeling and typical experimental errors. The fields would be greater at higher intensities, which might lead to a detectable difference. This is in qualitative agreement with experimental results [12,14–16]. Pisani *et al.* [16] found that for roughly comparable parameters to those considered here, there was no detectable difference between results obtained with plastic and aluminum layers, but that when the intensity was increased by a factor of 10, the mean energy inferred with the plastic layer was lower than with the aluminum layer, in accord with our results. To ensure an identical fast electron source in both cases, a first layer of aluminum was always used. Key *et al.* and Wharton *et al.* [12] also report a lower mean energy for plastic than metal targets, and a lower mean energy for a lighter metal than a heavier metal, with similar absorptions, as expected from our results. However, this was for intensities up to 100 times higher than we considered, and the differences could also be due to differences in the laser interaction with the different materials, so no definite conclusions can be drawn from this apparent agreement. Another example of differences between different materials comes from the results of Hall *et al.* [14], where the transport of fast electrons in ordinary and shock compressed plastic was compared, using $K\alpha$ emission. These results were explained in terms of electric field inhibition, using the hybrid code, by Dimitri *et al.* [15]. However, this case is somewhat atypical as magnetic field inhibition normally dominates [19], as in the cases considered here. The two-temperature fast electron distribution and lack of low-energy electrons in the distribution inferred at large depths, though they have been frequently reported [7,10,11,13,26,29], cannot be considered as indicative of field generation, as they could be features of the fast electron generation. Another, more subtle, indication that field generation is significant could still come from the apparent two-temperature distribution. Calculating the mean number density of fast electrons generated (n_f) using the results obtained at small depths in Sec. IV and the equation

$$n_f = \frac{f_{abs} I}{v_f \langle K \rangle}, \tag{16}$$

where v_f is the mean fast electron velocity into the target, gives results of the order of 10^{28} m^{-3}. For the experiments being considered, the laser was absorbed in a plasma formed by the prepulse or rising edge of the main pulse, not directly by the solid, so the absorption occurred at a density less than or equal to the critical density of 10^{27} m^{-3} for a 1 μm wavelength. Thus, it is impossible for the electrons to have been generated with such a high number density.

Another important conclusion from our results is that the fast electron transport in the solid target will affect the laser interaction. The laser can only generate the large currents and numbers of fast electrons observed because a return cur-

rent is supplied from the target, therefore, the laser interaction is affected not only by the plasma conditions in the interaction region, but also in the region from which the return current must be drawn. In our modeling, the targets were unable to provide the required current, so a significant part of it was provided by the fast electrons themselves, and they would reinteract with the laser. This extends the region from which the return current is drawn. It would lead to material and time dependent effects in the laser interaction. An alternative to drawing electrons from the target is to accelerate ions into it, which may help to explain proton emission from the back of targets [27–29].

Using the hybrid code to determine the fast electron generation from experimental results is extremely difficult, as the results depend on the time and spatial dependence of the fast electron distribution function, the boundary conditions, and the resistivity and heat capacity of the target over an extended range of temperatures. These last two parameters are not well known. To calculate them theoretically implies complex, quantum mechanical calculations. Evaluating them experimentally is also not straightforward. It would thus seem sensible to attempt to avoid field generation when trying to determine the fast electron generation. This could be done by using dense, high atomic number targets, by compressing the target and by preheating the target to lower the resistivity. However, this becomes increasingly difficult at higher intensities, and creates the problem that the fast electron generation itself may also be changed. The best method of overcoming the uncertainties in the modeling is to consider the results from many different diagnostics, thus cutting down the number of possible interpretations. It is just such a combination of diverse results that provides conclusive evidence for field generation by fast electrons in solid targets.

ACKNOWLEDGMENT

This work was supported by a grant from the Fundação para a Ciência e a Tecnologia.

[1] *International Committee on Radiation Units Report No. 37* (ICRU, Bethesda, MD, 1984).

[2] R. B. Miller, *An Introduction to the Physics of Intense Charged Particle Beams* (Plenum Press, New York, 1982), Chap. 4.

[3] J. D. Hares, J. D. Kilkenny, M. H. Key, and J. G. Lunney, Phys. Rev. Lett. **42**, 1216 (1979).

[4] R. S. Marjoribanks, M. D. J. Burgess, G. D. Enright, and M. C. Richardson, Phys. Rev. Lett. **45**, 1798 (1980).

[5] W. Priedhorsky, D. Lier, R. Day, and D. Gerke, Phys. Rev. Lett. **47**, 1661 (1981).

[6] P. Gibbon and E. Förster, Plasma Phys. Controlled Fusion **38**, 769 (1996).

[7] S. J. Gitomer, R. D. Jones, F. Begay, A. W. Ehler, J. F. Kephart, and R. Kristal, Phys. Fluids **29**, 2679 (1986).

[8] M. Tabak, J. M. Hammer, M. E. Glinsky, W. L. Kruer, S. C. Wilks, and J. Woodworth, Phys. Plasmas **1**, 1626 (1994).

[9] T. Tan, G. H. McCall, and A. H. Williams, Phys. Fluids **27**, 296 (1984).

[10] F. N. Beg, A. R. Bell, A. E. Dangor, C. N. Danson, A. P. Fews, M. E. Glinsky, B. A. Hammel, P. Lee, P. A. Norreys, and M. Tatarakis, Phys. Plasmas **4**, 447 (1997).

[11] B. Luther-Davies, A. Perry, and K. A. Nugent, Phys. Rev. A **35**, 4306 (1987).

[12] M. H. Key, M. D. Cable, T. E. Cowan, K. G. Estabrook, B. A. Hammel, S. P. Hatchett, E. A. Henry, D. E. Hinkel, J. D. Kilkenny, J. A. Koch, W. L. Kruer, A. B. Langdon, B. F. Lasinski, R. W. Lee, B. J. MacGowan, A. MacKinnon, J. D. Moody, M. J. Moran, A. A. Offenberger, D. M. Pennington, M. D. Perry, T. J. Philips, T. C. Sangster, M. S. Singh, M. A. Stoyer, M. Tabak, G. L. Tietbohl, M. Tsukamoto, K. Wharton, and S. C. Wilks, Phys. Plasmas **5**, 1966 (1998); K. B. Wharton, S. P. Hatchett, S. C. Wilks, M. H. Key, J. D. Moody, V. Yanovsky, A. A. Offenberger, B. A. Hammel, M. D. Perry, and C. Joshi, Phys. Rev. Lett. **81**, 822 (1998).

[13] G. Pretzler, Th. Schlegel, E. Fill, and D. Eder, Phys. Rev. E **62**, 5618 (2000).

[14] T. A. Hall, S. Ellwi, D. Batani, A. Bernardinello, V. Masella, M. Koenig, A. Benuzzi, J. Krishnan, F. Pisani, A. Djaoui, P. Norreys, D. Neely, S. Rose, M. H. Key, and P. Fews, Phys. Rev. Lett. **81**, 1003 (1998).

[15] D. Batani, J. R. Davies, A. Bernardinello, F. Pisani, M. Koenig, T. A. Hall, S. Ellwi, P. Norreys, S. Rose, A. Djaoui, and D. Neely, Phys. Rev. E **61**, 5725 (2000).

[16] F. Pisani, A. Bernardinello, D. Batani, A. Antonicci, E. Martinolli, M. Koenig, L. Gremillet, F. Amiranoff, S. Baton, J. Davies, T. Hall, D. Scott, P. Norreys, A. Djaoui, C. Rousseaux, P. Fews, H. Bandulet, and H. Pepin, Phys. Rev. E **62**, R5927 (2000).

[17] M. E. Glinsky, Phys. Plasmas **2**, 2796 (1995).

[18] A. R. Bell, J. R. Davies, S. Guerin, and H. Ruhl, Plasma Phys. Controlled Fusion **39**, 653 (1997).

[19] J. R. Davies, A. R. Bell, M. G. Haines, and S. M. Guerin, Phys. Rev. E **56**, 7193 (1997).

[20] A. R. Bell, J. R. Davies, and S. M. Guerin, Phys. Rev. E **58**, 2471 (1998).

[21] J. R. Davies, A. R. Bell, and M. Tatarakis, Phys. Rev. E **59**, 6032 (1999).

[22] S. M. Guerin, A. R. Bell, J. R. Davies, and M. G. Haines, Plasma Phys. Controlled Fusion **41**, 285 (1999).

[23] E. E. Fill, Phys. Plasmas **8**, 1441 (2001).

[24] M. Tatarakis, J. R. Davies, P. Lee, P. A. Norreys, N. G. Kassapakis, F. N. Beg, A. R. Bell, M. G. Haines, and A. E. Dangor, Phys. Rev. Lett. **81**, 999 (1998).

[25] M. Borghesi, A. J. Mackinnon, A. R. Bell, G. Malka, C. Vickers, O. Willi, J. R. Davies, A. Pukhov, and J. Meyer-ter-Vehn, Phys. Rev. Lett. **83**, 4309 (1999).

[26] L. Gremillet, F. Amiranoff, S. D. Baton, J. C. Gauthier, M. Koenig, E. Martinolli, F. Pisani, G. Bonnaud, C. Leborg, C. Rousseaux, C. Toupin, A. Antonicci, D. Batani, A. Bernardinello, T. Hall, D. Scott, P. Norreys, H. Bandulet, and H. Pepin, Phys. Rev. Lett. **83**, 5015 (1999).

[27] E. L. Clark, K. Krushelnick, J. R. Davies, M. Zepf, M. Tatar-

akis, F. N. Beg, A. Machacek, P. A. Norreys, M. I. K. Santala, I. Watts, and A. E. Dangor, Phys. Rev. Lett. **84**, 670 (2000).
[28] K. Krushelnick, E. L. Clark, M. Zepf, J. R. Davies, F. N. Beg, A. Machacek, M. I. K. Santala, M. Tatarakis, I. Watts, P. A. Norreys, and A. E. Dangor, Phys. Plasmas **7**, 2055 (2000).
[29] M. Zepf, E. L. Clark, K. Krushelnick, F. N. Beg, C. Escoda, A. E. Dangor, M. I. K. Santala, M. Tatarakis, I. F. Watts, P. A. Norreys, R. J. Clarke, J. R. Davies, M. A. Sinclair, R. D. Edwards, T. J. Goldsack, I. Spencer, and K. W. D. Ledingham, Phys. Plasmas **8**, 2323 (2001).
[30] C. W. Gardiner, *Handbook of Stochastic Methods*, 2nd ed. (Springer-Verlag, Berlin, 1985).
[31] C. K. Birdsall, and A. B. Langdon, *Plasma Physics via Computer Simulation* (McGraw-Hill, New York, 1985).
[32] D. S. Kershaw, J. Comput. Phys. **26**, 43 (1978).
[33] J. Yu, J. C. Kieffer, and A. Krol, Phys. Plasmas **6**, 1318 (1999).
[34] C. J. Joachain, *Quantum Collision Theory*, 3rd ed. (North-Holland, Amsterdam, 1987).
[35] H. M. Milchberg, R. R. Freeman, S. C. Davey, and R. M. More, Phys. Rev. Lett. **61**, 2364 (1988).
[36] A. R. Bell, Rutherford Appleton Laboratory Report RL-80-091, 1980 (unpublished).
[37] R. J. Harrach and R. E. Kidder, Phys. Rev. A **23**, 887 (1981).
[38] B. R. Wienke, J. Comput. Phys. **51**, 208 (1983).